Atmos. Chem. Phys., 8, 2741–2757, 2008
www.atmos-chem-phys.net/8/2741/2008/

Atmospheric Chemistry and Physics

Cloud system resolving model study of the roles of deep convection for photo-chemistry in the TOGA COARE/CEPEX region

M. Salzmann[1], **M. G. Lawrence**[1], **V. T. J. Phillips**[2], **and L. J. Donner**[3]

[1]Max-Planck-Institute for Chemistry, Department of Atmospheric Chemistry, PO Box 3060, 55020 Mainz, Germany
[2]Department of Meteorology, University of Hawaii at Manoa, 2525 Correa Road, Honolulu, HI 96822, USA
[3]Geophysical Fluid Dynamics Laboratory, NOAA, Princeton University, PO Box 308, Princeton, NJ 08542, USA

Received: 30 October 2007 – Published in Atmos. Chem. Phys. Discuss.: 10 January 2008
Revised: 7 May 2008 – Accepted: 7 May 2008 – Published: 22 May 2008

Abstract. A cloud system resolving model including photochemistry (CSRMC) has been developed based on a prototype version of the Weather Research and Forecasting (WRF) model and is used to study influences of deep convection on chemistry in the TOGA COARE/CEPEX region. Lateral boundary conditions for trace gases are prescribed from global chemistry-transport simulations, and the vertical advection of trace gases by large scale dynamics, which is not reproduced in a limited area cloud system resolving model, is taken into account. The influences of deep convective transport and of lightning on NO_x, O_3, and HO_x(=HO_2+OH), in the vicinity of the deep convective systems are investigated in a 7-day 3-D $248\times248\,km^2$ horizontal domain simulation and several 2-D sensitivity runs with a 500 km horizontal domain. Mid-tropospheric entrainment is more important on average for the upward transport of O_3 in the 3-D run than in the 2-D runs, but at the same time undiluted O_3-poor air from the marine boundary layer reaches the upper troposphere more frequently in the 3-D run than in the 2-D runs, indicating the presence of undiluted convective cores. In all runs, in situ lightning is found to have only minor impacts on the local O_3 budget. Near zero O_3 volume mixing ratios due to the reaction with lightning-produced NO are only simulated in a 2-D sensitivity run with an extremely high number of NO molecules per flash, which is outside the range of current estimates. The fraction of NO_x chemically lost within the domain varies between 20 and 24% in the 2-D runs, but is negligible in the 3-D run, in agreement with a lower average NO_x concentration in the 3-D run despite a greater number of flashes. Stratosphere to troposphere transport of O_3 is simulated to occur episodically in thin filaments in the 2-D runs, but on average net upward transport of O_3 from below ∼16 km is simulated in association with mean large scale ascent in the region. Ozone profiles in the TOGA COARE/CEPEX region are suggested to be strongly influenced by the intra-seasonal (Madden-Julian) oscillation.

Correspondence to: M. Salzmann
(salzmann@mpch-mainz.mpg.de)

1 Introduction

Tropospheric ozone is an important greenhouse gas and a key player in tropospheric chemistry. Over the remote tropical oceans deep convection rapidly moves O_3-poor air from the marine boundary layer (MBL) to the upper troposphere (UT) (e.g. Lelieveld and Crutzen, 1994; Wang et al., 1995; Kley et al., 1996; Pickering et al., 2001) while over polluted continental areas the transport of ozone and its precursors plays an important role for the upper tropospheric ozone budget (e.g. Dickerson et al., 1987; Pickering et al., 1990; Lawrence et al., 2003). Deep convection can also bring O_3-rich air from the lower stratosphere to the troposphere (e.g. Wang et al., 1995; Poulida et al., 1996; Stenchikov et al., 1996; Dye et al., 2000; Wang and Prinn, 2000) and air originating in the mid-troposphere is carried upwards in association with mid-level inflow into tropical squall lines (Scala et al., 1990) or mid-latitude storms (Wang and Chang, 1993). Furthermore, lightning NO_x can enhance O_3 production in deep convective outflow hundreds of kilometers downwind of deep convection (e.g. Pickering et al., 1990, 1993, 1996). In the troposphere, downward transport takes place in association with rear inflow into mesoscale convective systems (e.g. Scala et al., 1990; Salzmann et al., 2004). While Kley et al. (1997) argued that observed sharp ozone gradients indicate a lack of vertical

mixing across the tropopause, dry layers with high ozone mixing ratios are common in parts of the marine tropical troposphere and have been suggested to originate either from deep convection over continents lifting polluted air or from the stratosphere (Newell et al., 1996). In global chemistry-transport models, deep convective transport, which is typically parameterized using simplistic mass flux approaches, constitutes a major source of uncertainty (Mahowald et al., 1995; Lawrence and Rasch, 2005).

Wang and Prinn (2000) studied a CEPEX storm (CEPEX: Central Equatorial Pacific Experiment; Ramanathan et al., 1993) using 2-D and 3-D cloud resolving model simulations including chemistry and found that downward transport of O_3-rich air in association with deep convection, which took place in thin filaments in their simulations, lead to increases in upper tropospheric O_3 mixing ratios in spite of the upward transport of O_3-poor air. They suggested O_3 loss due the reaction with lightning-produced NO in cloud anvil regions can help explain the occasionally observed layers with extremely low concentrations of O_3 in the upper troposphere. Furthermore, they found that a considerable fraction of lightning NO_x was photochemically converted to HNO_3 in the vicinity of the storms. This fraction decreased with increasing NO production from 28% in a 2-D sensitivity run with a fairly large NO production to 12% in a 2-D run with an extremely large NO production. At very high simulated NO_x concentrations they found NO_x loss to be HO_x limited. Although lightning is much less frequent over oceans than over land (e.g. Christian et al., 2003), lightning NO constitutes one of the most important sources of NO_x over the remote tropical oceans next to ship emissions and the thermal decomposition of peracetyl nitrate (PAN), which is advected over long distances at high altitudes and subsequently transported downwards. Large photochemical losses of lightning NO_x in the vicinity of the storms would therefore be important in spite of the large uncertainty still related to the amount of NO produced per flash. Globally, lightning has been shown to have an important impact on OH and the lifetime of methane (Labrador et al., 2004; Wild, 2007).

In this study we use a so-called cloud system resolving model setup including chemistry (CSRMC) in order to study the impact of multiple storms and mesoscale convective systems over a period of several days. Horizontal advection in and out of the domain is taken into account by specifying lateral boundary conditions for trace gases. Furthermore, the mean ascent in the domain (associated with the Hadley and Walker cell and the intra-seasonal oscillation), which is not reproduced by limited area cloud system resolving models, is taken into account as in Salzmann et al. (2004) based on mean vertical velocities derived from observations over the tropical West Pacific east of Papua New Guinea during TOGA COARE (Webster and Lukas, 1992; Ciesielski et al., 2003). Taking into account the mean ascent largely compensates the mass balancing mesoscale subsidence between clouds which would otherwise erroneously be forced to take place in the domain (Salzmann et al., 2004) and for example lead to a significant overestimate of the thermal decomposition of PAN. We focus on the following issues:

1. The influence of NO production by lightning on NO_x, O_3, and HO_x, and the sensitivity of the model results to the dimensionality (2-D or 3-D) of the model.

2. Deep convective ozone transport (especially with regard to implications for its treatment in global chemistry-transport models), and, closely related to this, the role of regional scale ozone transport and locally produced lightning NO_x in explaining ozone profiles in the TOGA COARE/CEPEX region.

We also discuss the ozone results in the light of very low upper tropospheric ozone concentrations observed during CEPEX (Kley et al., 1996, 1997). Unfortunately, chemistry and flash rate observations are not available for the episode (19–26 December 1992) simulated in this model sensitivity study. In order to constrain the simulated flash rates and for the discussion of our chemistry results, we instead rely on observations from nearby regions and/or at other times.

The CSRMC is described in the next section. In Sects. 3–5 results for NO_x, O_3, and HO_x are presented. The influence of the intra-seasonal (Madden Julian) oscillation (ISO) on ozone profiles is discussed in Sect. 6 based on output from the global Model of Atmospheric Transport and Chemistry - Max Planck Institute for Chemistry version (MATCH-MPIC, Lawrence et al., 1999b; von Kuhlmann et al., 2003, and references therein). The CSRMC simulated meteorology (similar to Salzmann et al., 2004) and details of the CSRMC such as the algorithms used for identifying updrafts and anvils in the lightning parameterization are described in the electronic supplement http://www.atmos-chem-phys.net/8/2741/2008/acp-8-2741-2008-supplement.pdf. Additional material providing a rather comprehensive view of the details of our simulations and a brief description of MATCH-MPIC is also found in the supplement.

2 Model description and setup

The meteorological component of the cloud system resolving model including photo-chemistry (CSRMC) is based on a modified height coordinate prototype version of the Weather Research and Forecasting (WRF) model (Skamarock et al., 2001). Modifications to the base model and the meteorological setup are largely identical to Salzmann et al. (2004) and are described in the electronic supplement http://www.atmos-chem-phys.net/8/2741/2008/acp-8-2741-2008-supplement.pdf (Sect. S1.1 and Sect. S1.2). A "background" $CH_4-CO-HO_x-NO_x$ tropospheric chemistry mechanism with additional reactions involving PAN (peroxy acetyl nitrate, $CH_3C(O)O_2NO_2$), and loss reactions of acetone (CH_3COCH_3) which is based on

the mechanism from MATCH-MPIC (von Kuhlmann et al., 2003) is used in the present study (Sect. S1.3). Photolysis rates are computed using the computationally efficient scheme by Landgraf and Crutzen (1998). A simple parameterization of the production of nitrogen oxide by lightning (see below) and a scheme for dry deposition over water (based on Ganzeveld and Lelieveld, 1995, and references therein) have been implemented in the CSRMC. For soluble trace gases the uptake into or onto, release from, transport together with, and mass transfer between different model categories of hydrometeors (cloud droplets, rain, small ice particles, graupel, and snow) are calculated as in Salzmann et al. (2007), see also Sect. S1.5. For HNO_3 and H_2O_2 ice uptake from the gas phase is taken into account (Sect. S1.6). Aqueous phase reactions are currently not explicitly included in the CSRMC, except for the hydrolysis reaction of N_2O_5. Dissociation reactions are, however, to some extent implicitly included via the use of "effective" Henry's law coefficients in the mass transfer equations (Sect. S1.5). The rate of change of the gas phase concentration of the i-th trace gas is:

$$\begin{aligned}\partial_t C_{i,g} = &- \nabla \cdot \left(\mathbf{v} C_{i,g}\right) + \partial_t C_{i,g}|_{\mathrm{vlsat}} + \partial_t C_{i,g}|_{\mathrm{lno}} \\ &+ \partial_t C_{i,g}|_{\mathrm{turb}} + \partial_t C_{i,g}|_{\mathrm{solu}} + \partial_t C_{i,g}|_{\mathrm{drydep}} \\ &+ \partial_t C_{i,g}|_{\mathrm{chem}} \end{aligned} \quad (1)$$

where ∂_t is the partial derivative with respect to time, $\mathbf{v}=(u, v, w)$ is the three dimensional wind vector, $\partial_t C_{i,g}|_{\mathrm{vlsat}}$ is the rate of change due to the vertical advection by the large scale vertical motion which is not reproduced by the CSRMC (Salzmann et al., 2004, see also Sect. S1.2), $\partial_t C_{i,g}|_{\mathrm{lno}}$ is the rate of NO production by lightning, $\partial_t C_{i,g}|_{\mathrm{turb}}$ is the rate of change due to turbulent mixing by sub-grid scale eddies (parameterized applying Smagorinsky's closure scheme, e.g. Takemi and Rotunno, 2003), $\partial_t C_{i,g}|_{\mathrm{solu}}$ is the uptake or release rate of soluble gases by or from hydrometeors in the liquid or ice phase (Sect. S1.6), $\partial_t C_{i,g}|_{\mathrm{drydep}}$ is the dry deposition rate, and $\partial_t C_{i,g}|_{\mathrm{chem}}$ is the rate of change due to gas phase chemical reactions. The advection of trace gases, of water vapor, and of hydrometeors in the liquid and ice phase is calculated using the monotonic algorithm by Walcek (2000).

Lateral boundary conditions for trace gases are derived from 3-hourly MATCH-MPIC output (see Sect. S2 and Sect. S8). In the 3-D run (LTN3D), the horizontal domain size is $248\times248\,\mathrm{km}^2$ and the horizontal resolution is 2 km. The vertical resolution is 500 m in the troposphere with increasing grid spacings above 19 km and a total of 46 levels up to 24707 m. A timestep of 8 s is used. In the 2-D runs (NOLTN, LTN1, LTN2, LTNWP, and LTNHWP), the horizontal domain extension is 500 km and the domain is oriented in East-West direction. The horizontal resolution is again 2 km and the vertical resolution is 350 m in the troposphere with a timestep of 5 s. The meteorological setup in the 2-D runs is identical to Salzmann et al. (2004), while the timestep and the vertical grid spacing were increased for the 3-D run. An overview of the meteorological results is presented in Sect. S3.

2.1 Simple lightning NO parameterization

Lightning NO production is parameterized as follows: As a first step, updrafts are localized by fitting rectangles in the horizontal plane enclosing areas where the vertical velocity exceeds $5\,\mathrm{m\,s}^{-1}$. This is achieved by recursively cutting larger rectangles into smaller rectangles until no new edges are found with $w_{\max}\leq5\,\mathrm{m\,s}^{-1}$ everywhere (for a more detailed description of the algorithm see Sect S1.4). For each updraft, a flash rate F_{PR} (in flashes per minute) is calculated from:

$$F_{PR}=\alpha\cdot5\cdot10^{-6}w_{\max}^{k}. \quad (2)$$

where $w_{\max}$ is the maximum vertical velocity in meters per second. Based on empirical relationships, Price and Rind (1992) derived an exponent of k=4.54, which is somewhat less than the model study based estimate of at least 6 by Baker et al. (1995). Pickering et al. (1998), who among other convective systems studied a squall line during TOGA COARE, used different values for different model simulated storms in order to obtain results comparable to observed flash rates. For their 2-D TOGA COARE simulation, they increased the exponent from 4.54 to 5.3. α is an empirical scaling factor which is adjusted to improve the agreement with available flash rate observations. For a mid-latitude supercell storm Fehr et al. (2004) applied a scaling factor of 0.26. Here, sensitivity studies using various exponents and scaling factors were conducted (Table 1, Sect. 3).

The ratio $Z=N_{\mathrm{IC}}/N_{\mathrm{CG}}$ of the number of intra cloud (IC) flashes to the number of cloud to ground (CG) flashes can either be prescribed in the CSRMC or estimated from the empirical relationship (Price and Rind, 1993):

$$\begin{aligned}Z=&\,0.021\,(\Delta h)^4-0.648\,(\Delta h)^3+7.493\,(\Delta h)^2 \\ &-36.54\,(\Delta h)+63.09\end{aligned} \quad (3)$$

for clouds with $\Delta h\geq5.5\,\mathrm{km}$, where $\Delta h=z_{ctw}-z_{0^\circ\mathrm{C}}$ is the vertical distance between the 0°C isotherm and the cloud top at the location of the maximum vertical updraft velocity (z_{ctw}). The cloud top height z_{ct} is defined for each vertical column as the level above which the sum of the mass mixing ratios of all hydrometeor categories $q_{\mathrm{totm}}=q_{\mathrm{cloud\,water}}+q_{\mathrm{rain}}+q_{\mathrm{ice}}+q_{\mathrm{graupel}}+q_{\mathrm{snow}}$ drops to below $0.01\,\mathrm{g\,kg}^{-1}$ in all overlying levels. For clouds with $\Delta h<5.5\,\mathrm{km}$ all flashes are assumed to be IC flashes based on the observation that very little lightning is produced by clouds with $\Delta h<5.5\,\mathrm{km}$ and that clouds produce almost exclusively IC flashes during their growth stage before they start producing CG flashes (Price et al., 1997; Pickering et al., 1998).

The vertical distribution of lightning channel segments is essentially that of DeCaria et al. (2000, 2005), i.e., CG

Table 1. Lightning NO sensitivity runs.

Label	molec CG[a]	molec IC[a]	α in Eq. (2)	k in Eq. (2)	N_{CG}[b]	N_{IC}[b]	Z[c]	P_{tot}[d] CG	P_{tot}[d] IC	P_{tot}[d]
LTN3D	10	5	0.06	4.5	1021	10644	10.43[e]	10.0	53.3	63.4
NOLTN	–	–	–	–	–	–	–	–	–	–
LTN1	10	5	1.0	5.0	176	1447	8.21[e]	1.8	7.2	9.0
LTN2	10	5	1.0	4.8	254	702	2.76	2.5	3.5	6.1
LTNWP	67[f]	6.7	1.0	4.8	254[h]	702	2.76	17.0	4.7	21.7
LTNHWP	300[g]	30	1.0	4.8	254	702	2.76	76.2	21.1	97.3

[a] 10^{25} molecules per flash.
[b] Number of flashes calculated for the 7-day TOGA COARE runs using Eq. (2).
[c] Ratio of number of IC flashes to number of CG flashes.
[d] Total NO production (10^{28} molecules).
[e] Diagnosed from calculated total flash numbers.
[f] Same as in LTN run of Wang and Prinn (2000), based on Price et al. (1997) who suggested $6.7 \cdot 10^{26}$ NO molecules per CG flash.
[g] Same as the LTNH case of Wang and Prinn (2000), based on Franzblau and Popp (1989).
[h] For comparison: Wang and Prinn (2000) calculated a total of about 750 flashes, out of which ∼210 were CG flashes for the first hours of a 30 h 2-D run with 1000 km horizontal domain length.

flash segments are assumed to have a Gaussian distribution and IC segments are assumed to have a bimodal distribution corresponding to a superposition of two Gaussian distributions. The pressure dependence of the NO production is taken into account. In the present study, the upper mode of the IC distribution is assumed to be centered at $z{=}z_{(-15)} + 0.8{\cdot}(z_{ctw} - z_{(-15)})$, where $z_{(-15)}$ is the altitude of the –15°C isotherm, thus allowing the altitude of the upper mode to vary depending on the growth stage of the cloud.

CG flashes are placed (horizontally) in the vertical grid column at the location of the maximum updraft velocity, which is consistent with Ray et al. (1987), who based on dual Doppler radar and VHF lightning observations found that in a multi-cell storm, lightning tended to coincide with the reflectivity and updraft core. Nevertheless, this assumption potentially leads to a small over-estimate of the upward transport of lightning NO_x. IC flashes are horizontally placed inside the previously identified anvil area in the vertical column where q_{totm} above $z_{(-15)}$ is largest and which is still located within 80 km of the maximum updraft.

For each system, the anvil is identified as follows: First all grid points in the entire domain with a cloud top height z_{ct} between z_{ctw}–1400 m and z_{ctw}+1400 m are flagged. Then, one grid point wide connections between flagged regions ("bridges") and single points ("bumps") on the edges of the flagged regions are removed. Finally, all the flagged points are identified which lie inside the region in which the column with the maximum updraft velocity is located, and which are less than 80 km away from this column (see Sect. S1.4 for details). This fairly simple method allows us to assign anvils to the convective systems which have previously been identified by fitting rectangles as described above.

In the 2-D runs lightning-produced NO is released into vertical columns of the same horizontal base area as in the 3-D run, i.e., 2 km×2 km. For numerical efficiency, lightning NO production is calculated every 56 s in the 3-D run and every 60 s in the 2-D runs. This choice to some extent mimics the discreteness of flashes at times when flash rates are low.

3 Lightning NO sensitivity runs

3.1 Flash rates

Lightning in the TOGA COARE region is relatively infrequent. Orville et al. (1997), for example, found the annual number of CG flashes per unit area in the TOGA COARE region for 1993 to be at least one order of magnitude lower than that observed close to the nearby Papua New Guinean islands. From a number of dedicated observations during TOGA COARE it is possible to estimate typical CG flash rates per storm and area densities of CG flashes. These estimates have been used to adjust the parameters in the flash rate parameterization Eq. (2). Large uncertainty exists, however, regarding the ratio $Z{=}N_{IC}/N_{CG}$. Furthermore, the number of molecules produced per flash is still uncertain. Here, we conduct a number of 2-D sensitivity runs with various assumptions regarding lightning NO production, in addition to a 3-D reference run (see Table 1). In the LTN3D reference run and the LTN1 run, Z is calculated using the

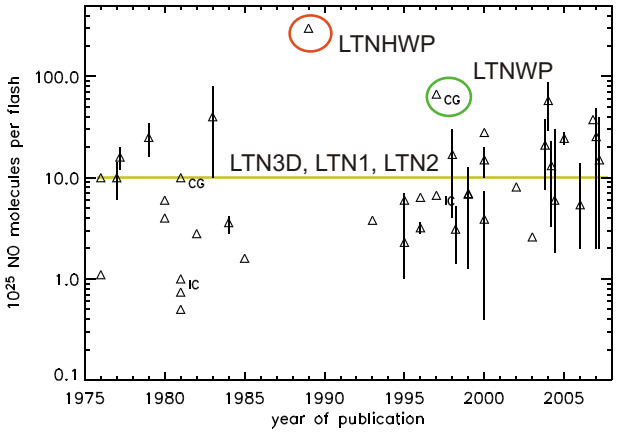

Fig. 1. Lightning NO production rates in molecules per flash from the literature based on Table 21 of Schumann and Huntrieser (2007).

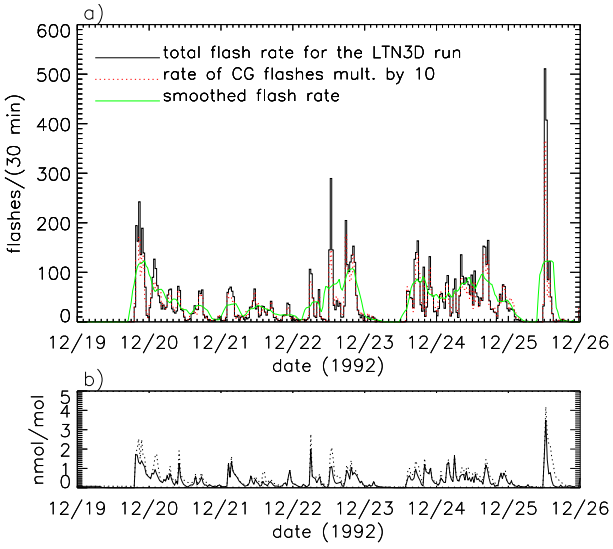

Fig. 2. (a) Flashes per 30 min in the LTN3D run and smoothed (5 point running mean) total flash rates (green line). **(b)** Maximum NO (solid line) and NO_x (dotted line) volume mixing ratios below ~16 km for the LTN3D run. Local 'solar' time is UTC plus 10.5 h.

parameterization in Eq. (3). In the other runs, Z=2.76 is prescribed for clouds with $\Delta h \geq 5.5$ km. The same value of Z has also been adopted by Wang and Prinn (2000) in their cloud resolving model study of a storm during CEPEX. Furthermore, in the LTNWP and the LTNHWP run we prescribe the same number of molecules per IC and per CG flash as Wang and Prinn (2000) in their LTN and LTNH sensitivity run, respectively. In our LTN3D, LTN1, and LTN2 run we adopt a lower NO production per CG flash (Fig. 1), but a greater ratio of molecules per IC flash to molecules per CG flash based on recent literature (Gallardo and Cooray, 1996; Cooray, 1997; DeCaria et al., 2000; Fehr et al., 2004).

Figure 2a shows modeled 30 min flash rates for the LTN3D run. The area density and maximum number of CG flashes in the LTN3D run are in line with the available observations. The daily area flash density in the TOGA COARE region can roughly be estimated to equal 0.0022 CG flashes per km^2 per day from Fig. 10 of Petersen et al. (1996) on days with high lightning activity during seasons with high lightning activity. The number of CG flashes in our LTN3D run is 1021 (Table 1) and the average area flash density during the last 6 days of the simulation (after the onset of deep convection in the model) is 0.0028 CG flashes per km^2 per day, which agrees with the observations within ~30%.

In selecting the parameters in the flash rate parameterization (Eq. 2) we attempted to approximatively match observed CG flash area densities as well as flash rates per storm. In severe continental thunderstorms rates of 20 and more flashes per minute can be sustained over an hour or more (see e.g. Skamarock et al., 2003; Fehr et al., 2004). In the TOGA COARE region, on the other hand, during more active storms flash rates of only 1–2 (and in one case 4) discharges (both IC and CG) per minute were observed by two NASA aircraft during storm overpasses (Orville et al., 1997). Lightning was only observed during 19 out of 117 storm overpasses. Petersen et al. (1996) also noted that the majority of convection over the tropical oceans does not produce lightning. For four cells with similar characteristics which were all observed on 15 February 1993 they found CG flash rates peaking at slightly above 7 CG flashes within 20 min (see their Fig. 5). Here, the maximum CG flash rates are typically between 10 and 20 flashes per 30 min in all lightning sensitivity runs (see Fig. 2a for the LTN3D, Fig. 3a for the LTN1 run, and Fig. 4a for the other 2-D lightning sensitivity runs). Often only the single most vigorous updraft significantly contributes to these rates (not shown).

3.2 Lightning NO_x

The maximum NO mixing ratios in the LTN3D run (Fig. 2b) fall largely within the range of available observations from the literature; several airborne observations of deep convective outflow in the Central and West Pacific yielded maximum NO mixing ratios of slightly below 1 nmol mol^{-1} (Huntrieser et al., 1998; Kawakami et al., 1997). In the outflow from continental thunderstorms, on the other hand, maximum NO mixing ratios of a few nmol mol^{-1} are not uncommon (e.g. Huntrieser et al., 1998). Only occasionally, the outputs from the LTN3D, LTN1, and LTN2 runs (Figs. 2b, 3b, and 4b) yield higher maxima than those observed over the Pacific. In the LTNWP and the LTNHWP (Figs. 4c and d) run we often find significantly higher maxima than observed. Somewhat higher maxima in the model are likely related to aircraft typically sampling deep convective outflow outside the region of maximum lightning activity. The extremely high NO maxima due to lightning in the LTNHWP

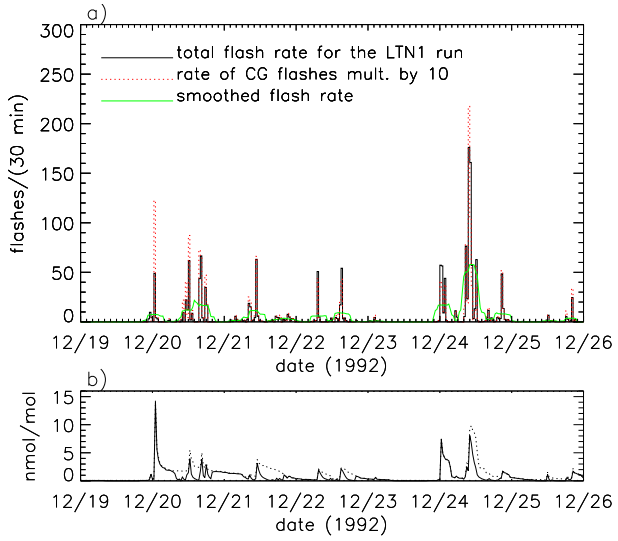

Fig. 3. Same as Fig. 2 for the LTN1 run.

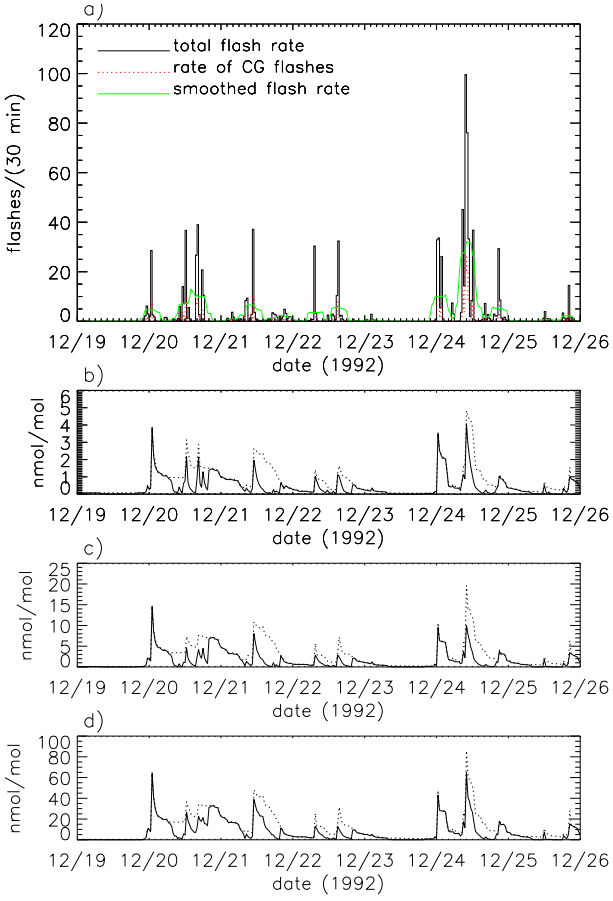

Fig. 4. **(a)** Same as Fig. 2a for the LTN2, the LTNWP, and the LTNHWP run. **(b-d)** Same as Fig. 2b for the LTN2, the LTNWP, and the LTNHWP run, respectively.

run can nevertheless be considered unrealistic.

Lower domain-average NO_x and NO volume mixing ratios in our LTNWP and LTNHWP runs compared to the volume mixing ratios at the end of the LTN and LTNH runs of Wang and Prinn (2000) (also included in Fig. 5) are in part caused by lower average flash rates in our study and the use of different model setups. Wang and Prinn (2000) used periodic lateral boundary conditions and calculated a total of about 750 flashes (estimated from their Fig. 6) out of which ∼210 were CG flashes for a 30 h run with a 1000 km 2-D domain; i.e. 0.17 CG flashes km^{-1} day^{-1} (compared to 0.07 CG flashes km^{-1} day^{-1} in the LTN2 run).

The scaling factor α in Table 1 is smaller for the 3-D run than for the 2-D run because of generally higher vertical velocities in 3-D simulations compared to 2-D simulations (Redelsperger et al., 2000; Phillips and Donner, 2006). In spite of the smaller α in the LTN3D run, the number of flashes and the number of NO molecules produced are greater in the LTN3D run than in the LTN1 run. Because of the different geometry, the domain-averaged mixing ratios in Fig. 5 are, nevertheless, higher in the LTN1 run; i.e. by assuming lightning-produced NO to be released into vertical columns of the same horizontal base area (2 km×2 km) in the 2-D runs as in the 3-D run, it is implicitly assumed that the horizontal "area" of the 2-D domain equals 2 km×500 km. For a given number of NO molecules produced by lightning, this leads to generally greater domain-average NO_x volume mixing ratios due to lightning in the 2-D simulations. Assuming a lower NO production per flash in the 2-D runs in order to compensate for this geometry effect, on the other hand, would also lead to unrealistic consequences for chemistry in the vicinity of the lightning NO source.

Using a vertical distribution of NO molecules which is constant except for being scaled by pressure for IC and CG flashes instead of the DeCaria et al. (2000) parameterization results in smaller maxima for the same number of NO molecules produced per flash (not shown), because of the two maxima in the vertical distribution by DeCaria et al. (2000) (compare also "lno" term in Fig. 8b). The influence of lightning on the average NO_x mixing ratio profiles is small in our 3-D run, but considerable in the 2-D runs (Fig. 5). An example of the spatial distribution of NO_x from the LTN3D run is shown in Fig. 6. An example from a 2-D run is shown in Fig. 7. Note, that this NO_x plume is almost completely advected out of the domain in ∼2.5–3 hours.

3.3 NO_x budget

In order to assess the influences of deep convection on chemistry in the model simulations we performed budget calculations. For each tendency on the right hand side of Eq. (1) we

define height dependent contributions by:

$$b_{\text{proc}}(z,t_1,t_2)=\frac{1}{XY}\int_0^X\int_0^Y\int_{t_1}^{t_2}\partial_t C_{i,g}|_{\text{proc}}\,dx\,dy\,dt \quad (4)$$

where X and Y is the horizontal extent of the domain in West-East and South-North direction, respectively. Horizontal advection $\partial_t C_{i,g}|_{\text{hadv}}=-\nabla\cdot\left(\mathbf{v}_h C_{i,g}\right)$ and vertical advection $\partial_t C_{i,g}|_{\text{vadv}}=-\partial_z\left(wC_{i,g}\right)$ (where $\mathbf{v}_h=(u,v)$ is the horizontal wind vector) are considered separately. The budget terms have been divided by time-averaged air density in order to express them in mixing ratio units. In addition to the "height resolved" terms in Eq. (4), the corresponding height integrated terms are analyzed for layers between z_1 and z_2:

$$B_{\text{proc}}=\int_{z_1}^{z_2} b_{\text{proc}}\,dz \quad (5)$$

Figure 8a shows NO_x mixing ratio profiles for the LTN3D run, and Fig. 8b shows time integrated domain-averaged tendencies. Most of the NO_x produced below 10 km is transported to the upper troposphere from where it is horizontally advected out of the domain (compare also Fig. 6 and Fig. 7). The lightning production term has two maxima reflecting the vertical distribution functions from DeCaria et al. (2000), in which IC as well as CG flashes contribute to the mid-tropospheric maximum while the upper tropospheric maximum is caused by IC flashes. Very little NO_x reaches the lowest kilometer of the atmosphere, a region where detrainment from deep cloud downdrafts can be expected. This result is consistent with a result of Pickering et al. (1998) from a CRM study of a single storm during TOGA COARE, who found only about 7.5% of the lightning-produced N mass in the lowest km because of the very weak downdrafts in their simulated storm. In mid-latitude storms they found considerably larger fractions. In the CSRMC, the downward transport could be underestimated because lightning NO is assumed to be produced in columns with maximum updraft velocities.

Net photochemical loss of NO_x within the domain plays a relatively much more important role in our 2-D lightning sensitivity runs than in our 3-D run (Fig. 9). Higher NO_x volume mixing ratios in the 2-D runs lead to increases of OH concentrations (Sect. 5) and a reduced chemical lifetime of NO_x. The fraction of NO_x photochemically lost within the domain varies between 20 and 24% in the 2-D runs, but is only 1% in the LTN3D run. In the 3-D run the loss of lightning-produced NO_x in the lower troposphere is in fact over-compensated by production from PAN. The net chemical production of NO_x is 2.0×10^{13} molecules cm^{-2} day^{-1} in the lower troposphere (LT, 0–5 km) during the last 6 days of the simulation, when deep convection is active. By far the largest chemical source of NO_x in the LT is PAN, while HNO_3 is the largest sink. PAN is horizontally advected into the domain above ~3 km. More details on the NO_x, PAN, and HNO_3 budgets can be found in the supplementary material http://www.atmos-chem-phys.net/8/2741/2008/acp-8-2741-2008-supplement.pdf.

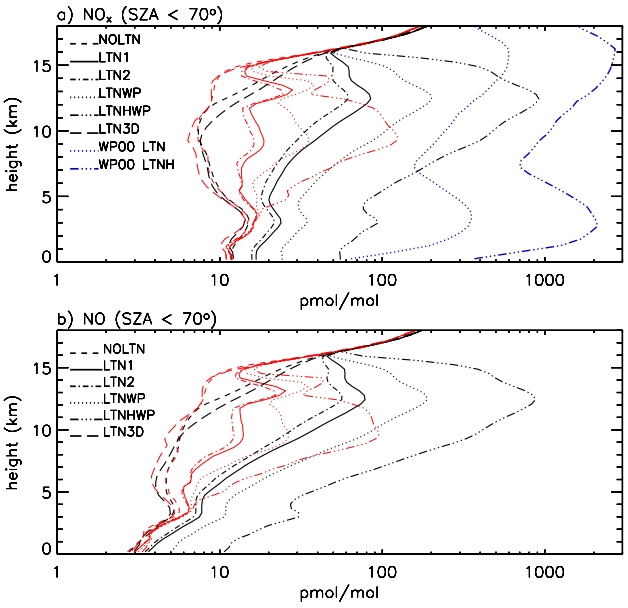

Fig. 5. Domain- and time-average (black lines) and median (red lines) volume mixing ratios of **(a)** NO_x and **(b)** NO for solar zenith angles (SZA) lower than 70°. Blue lines in (a): domain-averaged NO_x volume mixing ratio from Fig. 11 of Wang and Prinn (2000) at the end of their LTN and LTNH runs.

Comparable 2-D sensitivity runs with a pressure scaled but otherwise constant vertical distribution of NO molecules for IC and CG flashes yielded different fractions of NO_x lost within the domain (13–37%) and greater sensitivities to various assumptions regarding lightning NO_x production (Fig. 8.8 of Salzmann, 2005). In a non-HO_x-limited regime, the relatively smaller photochemical loss in the LTN3D run is in agreement with the lower average NO_x concentrations compared to the 2-D run. Furthermore, the shorter residence time in the 3-D domain probably also plays a role, but this is difficult to quantify.

4 Ozone

The sensitivity of the domain-averaged O_3 mixing ratios (Fig. 10a) to in situ lightning NO production is small and a moderate increase of ozone volume mixing ratios with increasing lightning NO production is simulated only in the mid-troposphere. The chemistry tendencies (shown in Fig. 10b) in percent per day in the NOLTN and the LTN3D run are similar to the ones calculated by Crawford et al. (1997) for their "low NO_x regime" (Table S6). They reflect the influence of lightning on ozone within the domain not taking into account ozone production further downwind. In the lower troposphere, the simulated O_3 mixing ratios are almost independent of the assumptions regarding lightning NO_x production, even in the sensitivity runs with very high

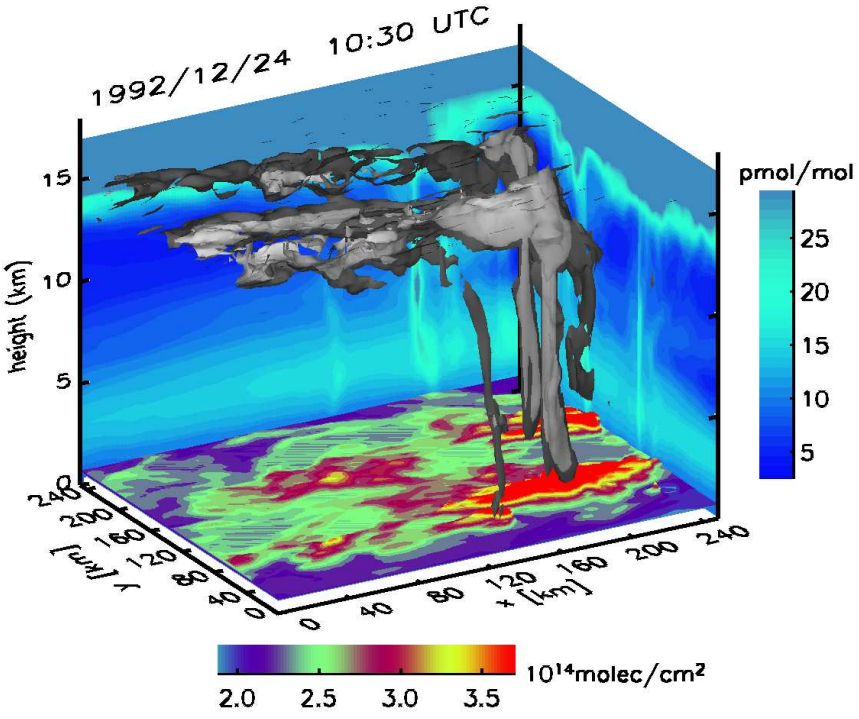

Fig. 6. Spatial distribution of NO_x in the LTN3D run for 24 December 1992, 10:30 UTC: 50 pmol mol^{-1} (dark gray, transparent) and 100 pmol mol^{-1} (light gray) isosurfaces, surface to 16 km column density contours (base area), and average volume mixing ratio in x (East-West) and y (South-North) direction (walls).

NO_x production by CG flashes. While here the sensitivity of local O_3 mixing ratios to in situ lightning NO_x production is small, Crawford et al. (1997) found considerably increased O_3 mixing ratios in air masses sampled during PEM-West B which had presumably been influenced by lightning over land upstream. These air masses had been more chemically aged and better mixed.

4.1 Ozone budget

The domain-averaged O_3 mixing ratios vary significantly during the LTN3D run (Fig. 11a) and are very similar to the boundary values (Fig. 11b), indicating that horizontal advection from the lateral boundaries rapidly influences and ultimately determines the simulated domain averages. Although vertical advection (Fig. 11e) tends to balance horizontal advection (Figs. 11d and 12b), the total tendency (Fig. 11c) mainly reflects horizontal advection from the boundaries. The time integrated total O_3 tendency (equaling ΔO_3 in Fig. 12), on the other hand, is smaller than the time integrated contributions from either horizontal or vertical advection, i.e., over longer time scales an approximate equilibrium ($\Delta O_3 \approx 0$) tends to establish. Furthermore, the contribution from photochemistry plays an important role in the 7-day integrated domain budget (Fig. 12). The most pronounced net loss takes place at ∼5 km where relatively O_3-rich air is advected into the domain and where photolysis rates are occasionally enhanced through sunlight reflected by mid-level cloud tops. While vertical advection of O_3-poor air on average tends to decrease O_3 volume mixing ratios above ∼14 km, vertical advection of ozone from the mid-troposphere (between ∼6–10 km) enhances O_3 mixing ratios between ∼10 and 14 km. This is consistent with our previous study of idealized tracer transport (Salzmann et al., 2004) in which we found considerable mid-tropospheric entrainment in a 3-D TOGA COARE simulation.

Horizontal advection plays a somewhat weaker role in determining the domain-average O_3 mixing ratios in the 2-D runs (Fig. 13) because of the larger 2-D domain and because meridional advection is not taken into account in the 2-D runs. Furthermore, in the LTN1 run the advection of O_3-poor air from below tends to decrease O_3 mixing ratios in the upper troposphere between ∼12 and 16 km (Fig. 14). The less obvious influence of mid-level entrainment in the 2-D run can be attributed to the weaker dependence on the lateral boundary values, i.e., horizontal layers of high O_3 mixing ratios in the mid-troposphere are more efficiently diluted by mixing in the 2-D runs. This is because in the 3-D run updrafts only cover a small part of the domain and only a part of the area downwind of the updrafts is directly affected. In 2-D runs, on the other hand, a single updraft influences the whole downwind part of the domain, and a significant frac-

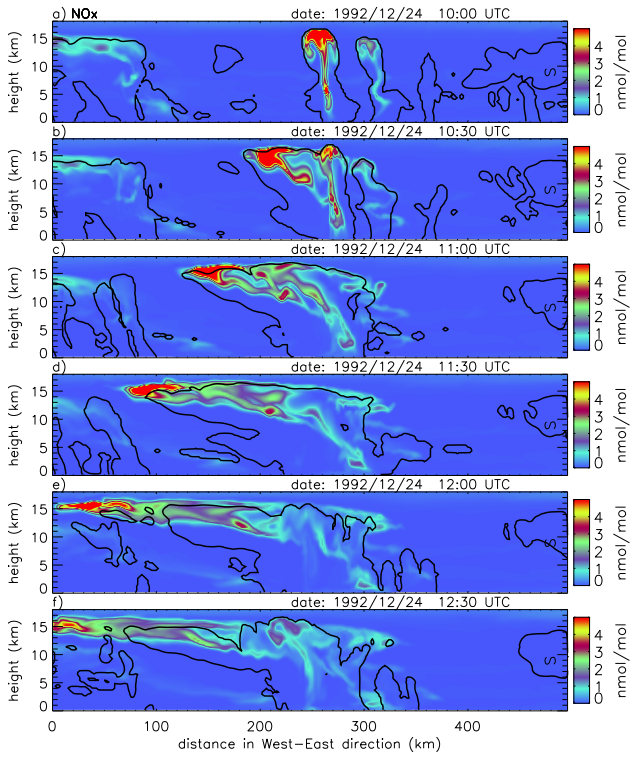

Fig. 7. NO_xvolume mixing ratios and the q_{totm}=0.01g kg^{-1} contour (where q_{totm}=$q_{cloud\,water}$ + q_{rain} + q_{ice} + $q_{graupel}$ + q_{snow} is the sum of all hydrometeor mass mixing ratios) during the development of a mesoscale convective system from 24 December 1992, 10:00 UTC to 24 December 1992, 12:30 UTC from the LTN1 run. The time increment between the plots in each of the panels is 30 min.

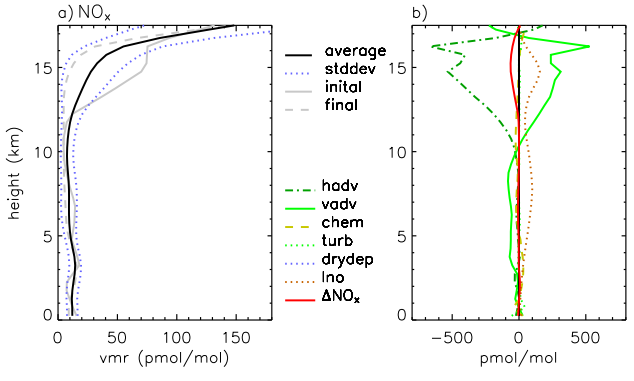

Fig. 8. **(a)** Time- and domain-averaged NO_x volume mixing ratio, averaged NO_x volume mixing ratio ± standard deviation, initial, and final NO_x volume mixing ratio profiles for the LTN3D run. **(b)** Budget terms (from Eq. (4), divided by the average air density) and the difference between the initial and the final profile (red line).

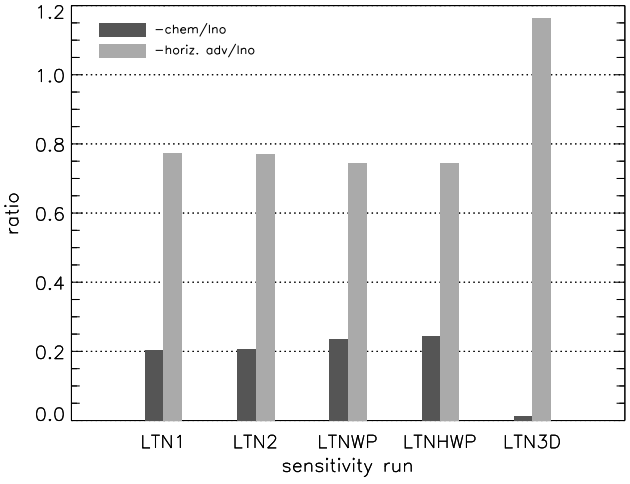

Fig. 9. Ratios of time integrated tropospheric column NO_x tendencies for the lightning sensitivity runs (calculated from Table S4).

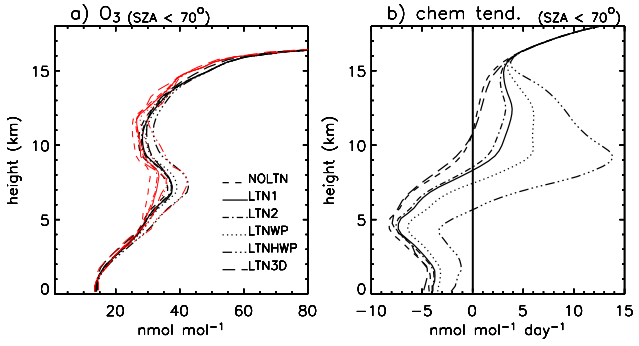

Fig. 10. **(a)** Domain- and time-averaged (black) and median (red) O_3 volume mixing ratio for SZA<70°. **(b)** Domain- and time-averaged net O_3 chemistry tendency for SZA<70°.

tion of the updrafts subsequently transports O_3-poor air to the upper troposphere. These updrafts do not pass through the mid-tropospheric high ozone layer, while in a 3-D simulation practically all updrafts can be expected to encounter such a layer at times when O_3-rich air is advected into the domain. Due to the greater fraction of updrafts in the 2-D runs which do not entrain O_3-rich air from the mid-troposphere, deep convective transport is on the whole less strongly affected by these layers in 2-D runs than in a 3-D run (compare Figs. 8c and 12b of Salzmann et al., 2004). In spite of these differences in transport, the lower tropospheric chemistry tendency is very similar in the LTN1 and the LTN3D run (Fig. 10b).

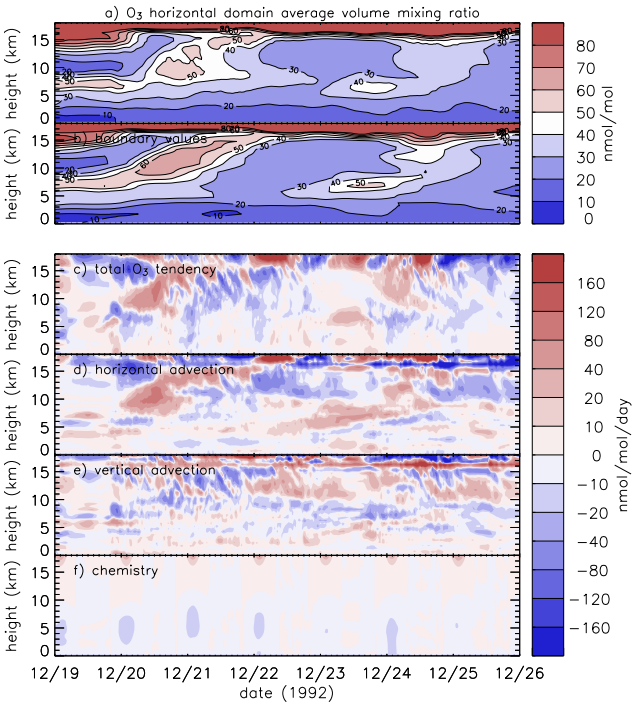

Fig. 11. **(a)** Time series of domain-averaged O_3 volume mixing ratios for the LTN3D run; **(b)** boundary values; **(c)**–**(f)** budget terms as defined by Eq. (4).

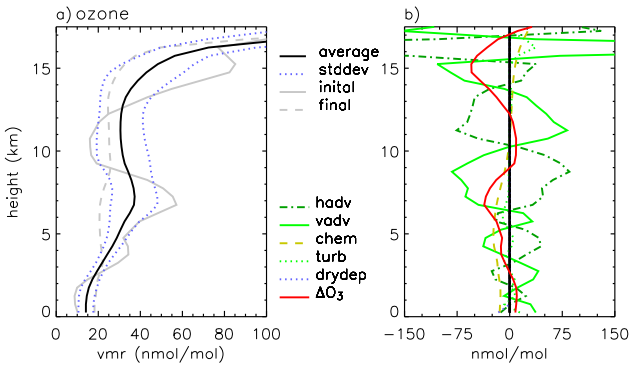

Fig. 12. As Fig. 8 for ozone.

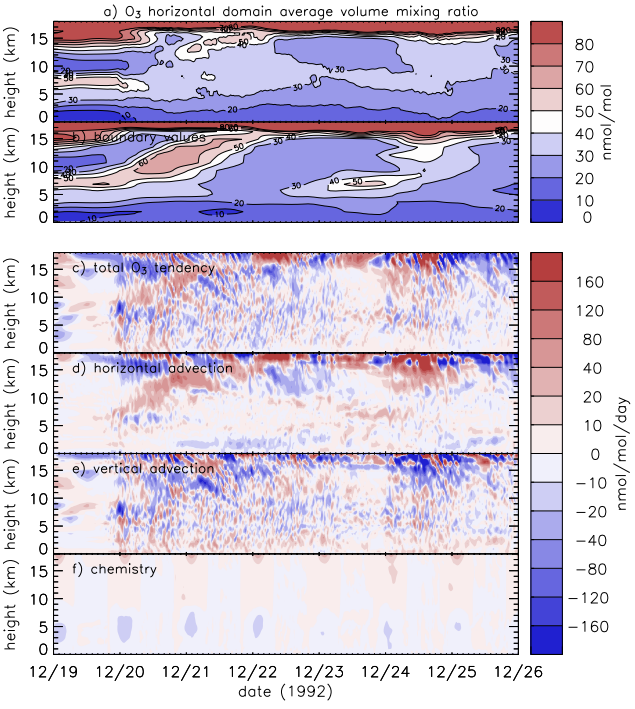

Fig. 13. As Fig. 11 for the LTN1 run.

4.2 Undiluted transport

Global and also mesoscale models often use bulk instead of ensemble mass flux parameterizations in order to calculate deep convective tracer transport, in which mid-level entrainment is incompatible with undiluted transport to the upper troposphere (Lawrence and Rasch, 2005). In Fig. 15, simulated upper tropospheric O_3 volume mixing ratio minima are compared to minima in the lowest model layer. The UT minimum in the LTN3D run is often much closer to the surface minimum than in the 2-D run, indicating that some undiluted air has reached the upper troposphere in this run in spite of significant mid-level entrainment (Sect. 4.1).

During the CEPEX cruise, extremely low (<5 nmol/mol) upper tropospheric O_3 volume mixing ratios were observed (e.g. Kley et al., 1996, 1997). A few model studies (Wang et al., 1995; Lawrence et al., 1999a) have reproduced these minima qualitatively, but not quantitatively. An exception has been the cloud resolving model study by Wang and Prinn (2000), who suggested that lightning related O_3 loss can help explain layers of very low O_3 in the upper tropical troposphere. Figure 15 shows pronounced decreases of O_3 mixing ratios indicating the loss of O_3 in the reaction with NO only for the LTNHWP run and to a much lesser extent also for the LTNWP run. Since the number of molecules per flash in the LTNHWP run is several times as large as the next largest estimate from the literature (Fig. 1), it is extremely unlikely that the occasionally observed layers of very low O_3 concentration are caused by lightning NO production.

In the present study a reproduction of the extremely low upper tropospheric O_3 concentrations observed during the CEPEX cruise was not to be anticipated since near-zero lower tropospheric O_3 volume mixing ratios can mainly be expected during the easterly phase of the intra-seasonal oscillation (see discussion in Sect. 6). Furthermore, the lifetime of O_3 in the MBL is of the order of few days and the lateral boundary conditions do not yield very low O_3 concentrations in either the upper or the lower troposphere. In order to

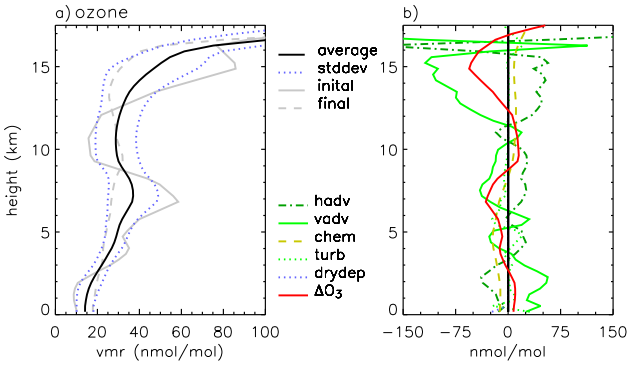

Fig. 14. As Fig. 12 for the LTN1 run.

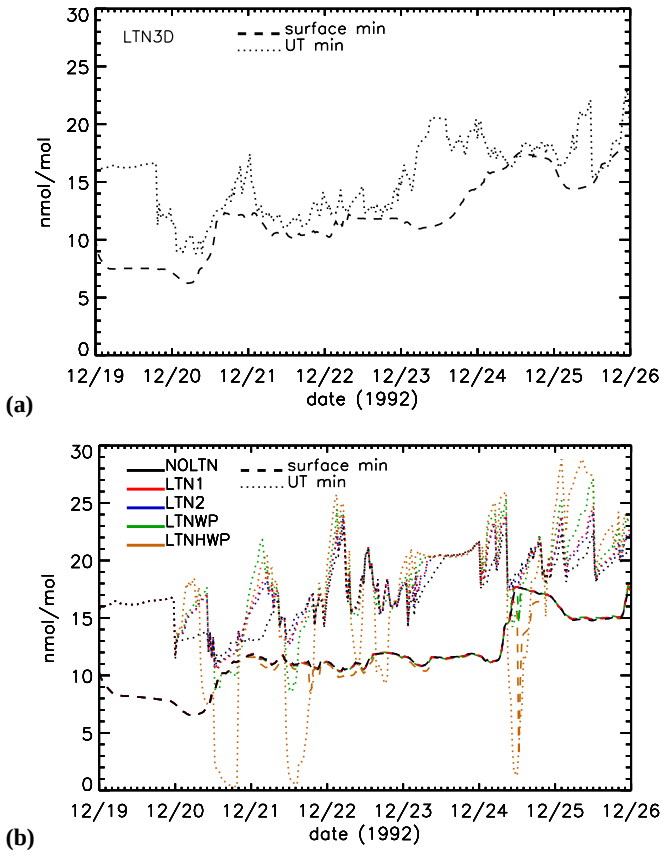

Fig. 15. Time series of minimum O_3 mixing ratios in the lowest model layer (dashed lines) and in the UT (defined from about 10 km to about 16 km, dotted lines) for **(a)** the LTN3D run and **(b)** the 2-D lightning sensitivity runs.

reproduce the very low ozone concentrations observed during CEPEX, one would most likely need a larger domain. Furthermore, as has been suggested in Kley et al. (1996); Lawrence et al. (1999a), it might be necessary to include additional reactions involving halogens (e.g. Davis et al., 1996; Sander and Crutzen, 1996, compare discussion in Sect. 6).

4.3 Small scale downward transport

Small scale downward transport of air with stratospheric origin in association with deep convection has been simulated in a number of two-dimensional cloud resolving model studies (Scala et al., 1990; Wang et al., 1995; Stenchikov et al., 1996; Wang and Prinn, 2000) in agreement with observations by Poulida et al. (1996) and Dye et al. (2000), who found air with stratospheric characteristics in the upper troposphere in the vicinity of mid-latitude storms. A very pronounced example from our LTN1 run is shown in Fig. 16 where O_3-rich air is advected downward in the rear inflow of a large mesoscale convective system. In the LTN3D run, such events are less easily identified, in part possibly due to the lower vertical resolution. Newell et al. (1996, 1999) interpreted thin horizontal layers in the troposphere as frozen signatures of the transfer of boundary layer air into the free troposphere or of stratospheric air into the troposphere. Newell et al. (1996) identified over 500 layers with a mean thickness of about 400 m from 105 vertical profiles sampled during PEM-West A over the West Pacific. They found these layers to extend over distances of 100–200 km or more. Using a different method to identify horizontal layers, Newell et al. (1999) found the average thickness of horizontal layers during PEM-West A to be about 800 m. The vertical resolution in this study is not high enough to adequately resolve the thinner ones among these layers. Instead, we focus on a comparison with Wang and Prinn (2000), who found that downward transport of O_3-rich air increased upper tropospheric O_3 mixing ratios, outweighing the effect of upward transport of O_3-poor air. In the LTN1 run, on the other hand, vertical advection tends to decrease upper tropospheric O_3 mixing ratios (Fig. 14). On the whole, a small net amount of O_3 is transported from below 16 km (troposphere) to above 16 km (stratosphere) in our simulations: 4×10^{15} molecules cm^{-2} day^{-1} in the LTN3D run, and 6×10^{15} molecules cm^{-2} day^{-1} in the LTN1 run. This small upward transport is influenced by the method used to specify the large scale forcing (see Sect. S5.3 for details) and is consistent with parts of the tropics being a region of average lower stratospheric ascent and troposphere to stratosphere transport (Holton et al., 1995; Corti et al., 2005).

The reason why Wang and Prinn (2000) found downward transport to increase upper tropospheric O_3 mixing ratios in spite of the upward transport of O_3-poor air might best be explained by their initial profile, which varied by only $\sim$3–4 nmol mol^{-1} between the surface and the upper troposphere, so that the upward transport of O_3-poor air played a relatively smaller role. In order to better quantify the influences of small scale downward transport on upper tropospheric O_3 concentrations in the tropics, additional detailed observations of O_3 and anthropogenic pollutants in

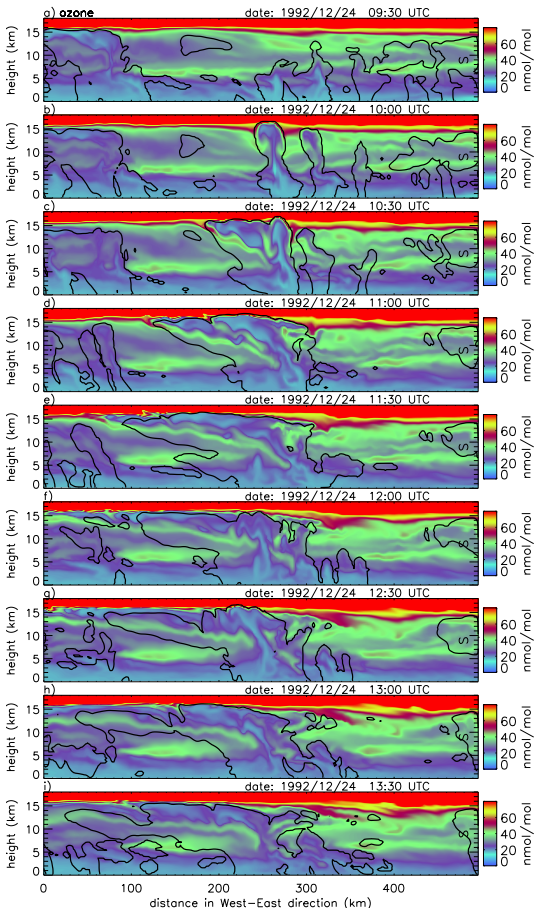

Fig. 16. O_3 volume mixing ratios (filled) from the LTN1 run for 24 December 1992, 9:30 UTC to 13:30 UTC and total hydrometeor mixing ratio q_{totm}=0.01g kg^{-1} contour.

the vicinity of deep convection are necessary that allow us to discriminate between vertical transport from below and import from the stratosphere, in combination with dedicated 3-D model studies, possibly using an idealized O_3 tracer and very high vertical resolution.

5 HO_x

Together with NO_x, hydrogen oxides play a crucial role for the troposphere's oxidation capacity and ozone chemistry. Figure 17 shows increasing OH concentrations with increasing lightning NO production in the 2-D lightning sensitivity runs and slightly decreasing HO_x concentrations in all runs but the LTNHWP run, in which the decrease is somewhat larger (of the order of a few pmol mol^{-1} in the upper troposphere). An increase of OH and a small decrease of HO_2 is caused by the NO oxidation reaction

$$NO + HO_2 \rightarrow NO_2 + OH$$

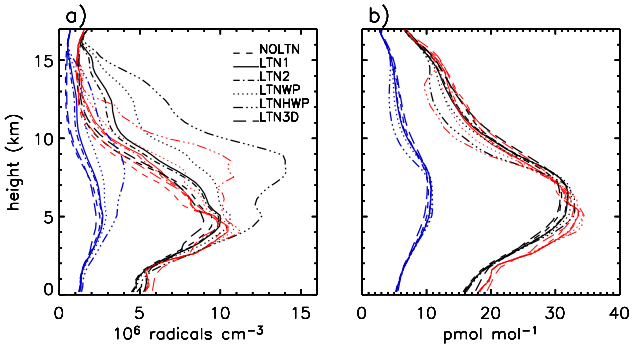

Fig. 17. (a) Median (red) and average (black lines) OH concentration around local noon and diurnal averages (blue). **(b)** Same for HO_x volume mixing ratios.

which shifts the partitioning between OH and HO_2 towards higher OH/HO_2 ratios while leaving the HO_x concentration constant. At very high NO concentrations in the vicinity of the flashes HO_x concentrations decrease due to the termination reaction of OH with NO_2 in which HNO_3 is formed. While we find increasing OH concentrations with increasing lightning NO production, Wang and Prinn (2000) found a very strong decrease of OH in one of their lightning sensitivity runs and a complete depletion of OH throughout the troposphere in the other run, which is consistent with significantly higher NO_x concentrations in their simulations (Fig. 5). The elevated HO_x concentrations above the boundary layer in Fig. 17 are caused by larger scale horizontal transport of O_3-rich air (compare Sect. 4 and Sect. 6). Elevated OH concentrations above the boundary layer have previously been observed above the eastern tropical Pacific under conditions of high NO_x and CO concentrations at these altitudes (Davis et al., 2001).

6 Role of the intra-seasonal oscillation (ISO) for ozone profiles

Kley et al. (1996, 1997) found extremely low O_3 mixing ratios during CEPEX either in the lower or the upper troposphere (depending on wind direction), but not in the upper and the lower troposphere at the same time. Figure 18 suggests that the surface concentrations of O_3, CO, and NO_x from MATCH-MPIC are strongly influenced by the phase of the intra-seasonal (Madden-Julian) oscillation (ISO, e.g. Madden and Julian, 1994) as reflected by the 10 m zonal wind. During the westerly phase (WP), relatively O_3, CO, and NO_x-rich air is found in the lowest model layer. While the zonal wind velocity in the MBL (below ~1000 m) is positively correlated with minimum O_3 volume mixing ratios in the MBL just south of the Equator between 150°E and 180°E (Fig. 19a), upper tropospheric minimum O_3 volume mixing ratios are negatively correlated with the zonal wind velocity in the MBL (Fig. 19b); i.e., during the WP,

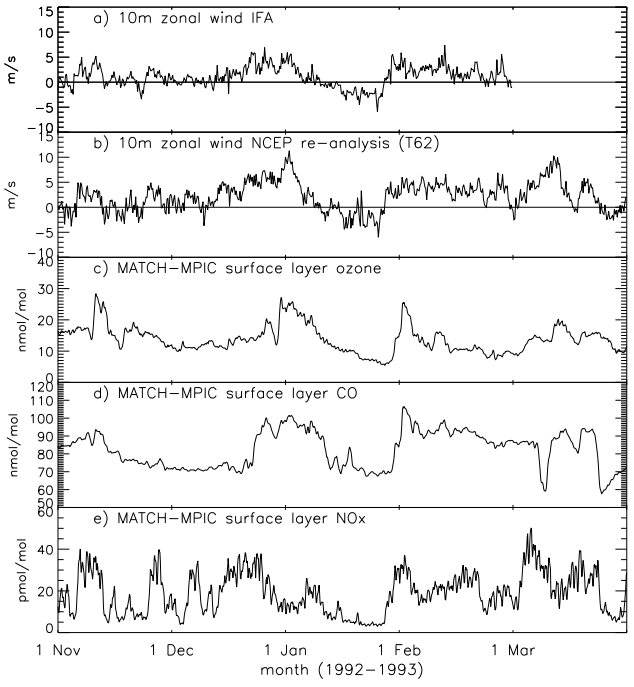

Fig. 18. Time series of **(a)** 10 m observed zonal wind, **(b)** 10 m zonal wind from the interpolated NCEP re-analysis data (see Sect. S8), **(c)** O_3 volume mixing ratio in the lowest model layer (surface layer) calculated by MATCH-MPIC, **(d)** surface layer CO, **(e)** surface layer NO_x at the site of the TOGA COARE IFA.

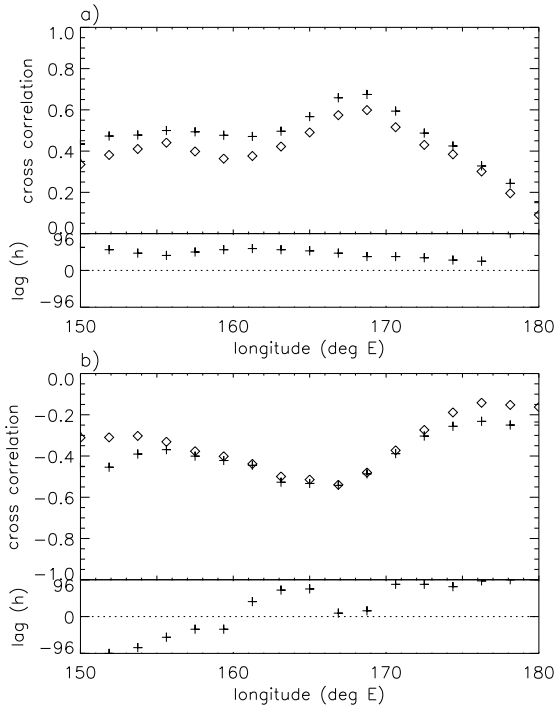

Fig. 19. Upper panels: Correlation of vertically averaged zonal wind velocity below ∼1000 m to **(a)** minimum O_3 volume mixing ratios in the MBL (below ∼1000 m) and **(b)** minimum O_3 volume mixing ratios in the upper troposphere (∼10–15 km), at 2.86°S for 31 October 1992 to 31 March 1993 from MATCH-MPIC for lag 0 h (diamonds) and for a lag between –96 and 96 h (lower panels) at the time of the maximum absolute correlation (crosses).

O_3 volume mixing ratios in the MBL tend to be higher and upper tropospheric O_3 volume mixing ratios lower than during the easterly phase. The zonal wind component lags O_3 in the MBL (Fig. 19a, lower panel), but taking into account a lag does not improve the correlation significantly at most longitudes. The increase in lower tropospheric O_3 volume mixing ratios during the WP is most likely related to cross-equatorial flow over the Indonesian Archipelago advecting polluted air masses from the Northern Hemisphere into the TOGA COARE/CEPEX region (see schematic in Fig. 20). This cross-equatorial flow is characteristic of the westerly phase of the ISO (e.g. Yanai et al., 2000; McBride et al., 1995). While surface winds are westerly during the WP, upper tropospheric winds tend to be easterly, advecting O_3-poor air from convective regions of the central Pacific into the region. During the easterly phase of the ISO the flow is roughly opposite. The dependence of O_3 concentrations on the phase of the ISO and regional scale horizontal advection can help to explain the lack of coincidence between upper tropospheric and lower tropospheric O_3 minima in the profiles observed during CEPEX. Furthermore, one could speculate that the low (high) NO_x regime (in the upper troposphere) identified by Crawford et al. (1997) might coincide with the westerly (easterly) phase of the ISO. The seven-day episode from 19–26 December 1992 is characterized by the onset of a strong WP.

MATCH-MPIC reproduces the ozone minima observed during CEPEX qualitatively but not quantitatively (Lawrence et al., 1999a); a possible candidate for a missing chemical ozone sink in the model being halogen-catalyzed ozone destruction (e.g. Davis et al., 1996; Sander and Crutzen, 1996).

The domain of the CSRMC is too small to simulate the regional scale transport associated with the ISO explicitly; instead the effect of regional scale horizontal advection is taken into account by specifying boundary conditions for trace gases. In the future, growing computer power will allow us to increase domain sizes and a multiply-nested cloud resolving model setup including chemistry for TOGA COARE will become feasible. A nested setup without chemistry is currently being evaluated for TOGA COARE.

7 Summary and conclusions

A cloud system resolving model including a simple lightning NO parameterization has been developed which allows us to study the influences of multiple storms and mesoscale convective systems on tropospheric chemistry in the TOGA COARE/CEPEX region over a period of several days. In situ lightning NO production is simulated to have a minor impact

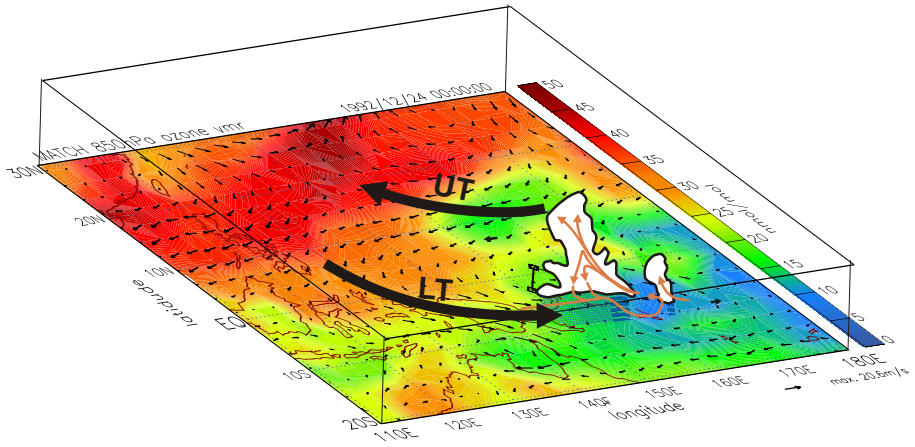

Fig. 20. Schematic: During the westerly phase of the ISO lower tropospheric cross-equatorial flow transports polluted air to the TOGA COARE/CEPEX region. The contours at the base are 850 hPa ozone volume mixing ratios from MATCH-MPIC and interpolated wind vectors are from the NCEP re-analysis dataset for 24 December 1992, 00:00 UTC.

on domain-averaged O_3, and the lightning NO_x plumes are horizontally advected out of the domain. The effect of lightning NO on domain-averaged NO_x strongly depends on the dimensionality of the model. In the 3-D reference (LTN3D) run lightning has a weak influence on the domain-average NO_x profile, but in the 2-D sensitivity runs lightning NO causes a large increase of domain-averaged NO_x because of the smaller implicitly assumed "volume" of the 2-D domain. Significantly lower NO_x volume mixing ratios in the LTN3D run, in spite of a much higher number of flashes, have an important implication for the loss of NO_x in the vicinity of the storms: While between 20 and 24% of the lightning-produced NO_x is lost due to chemistry inside the domain in the 2-D runs, this fraction is negligible in the LTN3D run and the loss is more than compensated by NO_x production from PAN. This suggests that the results of 2-D sensitivity runs are to be interpreted with caution and that 3-D runs are needed in order to realistically assess the influences of in situ lightning on local chemistry. Because multi-day 3-D runs are still computationally expensive (to our knowledge this is the first multi-day cloud system resolving study including chemistry), 2-D sensitivity runs can nevertheless be useful, especially for comparing with 2-D sensitivity runs from a previous study. Domain-averaged OH is found to increase with increasing lightning NO production and HO_x is fairly insensitive except for a notable decrease in the run with extremely high NO production per flash.

Mid-level entrainment plays an important role for O_3 transport from the mid-troposphere to the UT between ∼10 and 14 km, but transport of O_3-poor air from the MBL tends to decrease O_3 volume mixing ratios between 14 and 15.5 km in the LTN3D run. In spite of the importance of mid-level entrainment, undiluted O_3-poor air from the MBL reaches the upper troposphere more frequently in this run than in the 2-D runs, indicating the presence of undiluted convective cores (e.g. Heymsfield et al., 1978). Unlike in a bulk updraft cumulus transport parameterization or single column model, mid-level entrainment does not preclude the transport of undiluted air in a cloud system model since the dynamics of multiple storms and mesoscale convective systems is modeled. The finding of undiluted transport despite mid-level entrainment strongly suggests that plume ensemble parameterizations (e.g. Arakawa and Schubert, 1974; Gidel, 1983; Donner, 1993; Lawrence and Rasch, 2005) should be used instead of bulk mass flux parameterizations in global chemistry-transport models.

The causes of extremely low O_3 mixing ratios in the upper troposphere were examined through a series of sensitivity studies. We found that low O_3 mixing ratios can be a result of lightning-produced NO when high NO production rates and flash rates are used in a 2-D run, similar to Wang and Prinn (2000). However, a recent review of NO production by lightning (Schumann and Huntrieser, 2007) indicates that the NO production rate used in this sensitivity simulation is 10–100 times greater than most values reported in the literature. We therefore think this source is unrealistic.

We find vertical transport of ozone poor air to play a larger role in causing low upper tropospheric mixing ratios than Wang and Prinn (2000), who specified an initial O_3 profile with a relatively small vertical gradient between the boundary layer and the upper troposphere.

A reproduction of the extremely low O_3 concentrations observed during CEPEX (which started in the TOGA COARE region) was not to be anticipated in the present study since during the westerly phase of the intra-seasonal oscillation (ISO), relatively O_3-rich air is transported to the region by low level westerlies. Correlations between zonal wind and ozone volume mixing ratios from MATCH-MPIC for

31 October 1992 to 31 March 1993 suggest that vertical ozone profiles in the TOGA COARE/CEPEX region are strongly influenced by the ISO. This influence can help to explain the lack of coincidence between upper and lower tropospheric O_3 minima observed during CEPEX.

In the LTN1 run, small scale downward transport of ozone from the tropopause layer is simulated to occur in thin filaments extending far into the troposphere in association with rear inflow into mesoscale convective systems. On the whole, however, vertical advection tends to decrease upper tropospheric ozone mixing ratios in this run due to the upward transport of O_3-poor air from the MBL, and a small average net upward transport of O_3 from below $\sim$16 km in association with average large scale ascent is simulated in all runs. In order to better quantify the influences of small scale downward transport, additional observations in the vicinity of deep convection are necessary as well as dedicated 3-D model studies with very high vertical resolution. Since cloud system resolving model simulations require meteorological input from comprehensive observation campaigns such as TOGA COARE nested cloud resolving model simulations are likely to be a good alternative in many regions. Furthermore, as discussed in Salzmann et al. (2004), the application of observation derived large scale forcings for trace gases would, unlike for water vapor and potential temperature, be problematic.

Acknowledgements. We are very thankful to Larry Horowitz for providing pre-processed NCEP meteorological data for MATCH-MPIC input and to Rolf von Kuhlmann for useful discussions and advice on the chemistry mechanism and the implementation of the ice uptake. Furthermore, we appreciate the comments by two referees which have led to many significant improvements of our initial manuscript. This research was supported by funding from the German Research Foundation (DFG) Collaborative Research Centre 641 (SFB 641) "The Tropospheric Ice Phase (TROPEIS)" and from the German Ministry of Education and Research (BMBF), project 07-ATC-02. The model output files in netCDF format ($\sim$180Gb in total) can be obtained upon request from the authors at the MPI-C.

Edited by: Ronald Cohen

References

Arakawa, A. and Schubert, W. H.: Interaction of a cumulus cloud ensemble with the large-scale environment, Part I, J. Atmos. Sci., 31, 674–701, 1974.

Baker, M. B., Christian, H. J., and Latham, J.: A computational study of the relationships linking lightning frequency and other parameters, Q. J. R. Meteorol. Soc., 121, 1525–1548, 1995.

Christian, H. J., Blakeslee, R. J., Boccippio, D. J., Boeck, W. L., Buechler, D. E., Driscoll, K. T., Goodman, S. J., Hall, J. M., Koshak, W. J., Mach, D. M., and Stewart, M. F.: Global frequency and distribution of lightning as observed from space by the Optical Transient Detector, J. Geophys. Res., 108, 4005, doi:10.1029/2002JD002347, 2003.

Ciesielski, P. E., Johnson, R. H., Haertel, P. T., and Wang, J.: Corrected TOGA COARE sounding humidity data: Impact on diagnosed properties of convection and climate over the warm pool, J. Climate, 16, 2370–2384, 2003.

Cooray, V.: Energy dissipation in lightning flashes, J. Geophys. Res., 102, 21 401–21 410, 1997.

Corti, T., Luo, B. P., Peter, T., Vömel, H., and Fu, Q.: Mean radiative energy balance and vertical mass fluxes in the equatorial upper troposphere and lower stratosphere, Geophys. Res. Lett., 32, L06802, doi:10.1029/2004GL021889, 2005.

Crawford, J. H., Davis, D. D., Chen, G., Bradshaw, J., Sandholm, S., Kondo, Y., Merill, J., Liu, S., Browell, E., Gregory, G., Anderson, B., Sachse, G., Barrick, J., Blake, D., Talbot, R., and Pueschel, R.: Implications of large shifts in tropospheric NO_x levels in the remote tropical Pacific, J. Geophys. Res., 102, 28 447–28 468, 1997.

Davis, D., Crawford, J., Liu, S., McKeen, S., Bandy, A., Thornton, D., Rowland, F., and Blake, D.: Potential impact of iodine on tropospheric levels of ozone and other critical oxidants, J. Geophys. Res., 101, 2135–2147, 1996.

Davis, D., Grodzinsky, G., Chen, G., Crawford, J., Eisele, F., Mauldin, L., Tanner, D., Cantrell, C., Burne, W., Tan, D., Faloona, I., Ridley, B., Montzka, D., Walega, J., Grahek, F., Sandholm, S., Sachse, G., Vay, S., Anderson, B., Avery, M., Heikes, B., Snow, J., O'Sullivan, D., Shetter, R., Lefer, B., Blake, D., Blake, N., Carroll, M., and Wang, Y.: Marine latitude/altitude OH distributions: Comparison of Pacific Ocean observations with models, J. Geophys. Res., 106, 32 691–32 708, 2001.

DeCaria, A. J., Pickering, K. E., Stenchikov, G. L., Scala, J. R., Stith, J. L., Dye, J. E., Ridley, B. A., and Laroche, P.: A cloud-scale model study of lightning-generated NO_x in an individual thunderstorm during STERAO-A, J. Geophys. Res., 105, 11 601–11 616, 2000.

DeCaria, A. J., Pickering, K. E., Stenchikov, G. L., and Ott, L. E.: Lightning-generated NO_x and its impact on tropospheric ozone production: A three-dimensional modeling study of a Stratosphere-Troposphere Experiment: Radiation, Aerosols and Ozone (STERAO-A) thunderstorm, J. Geophys. Res., 110, D14303, doi:10.1029/2004JD005556, 2005.

Dickerson, R. R., Huffman, G. J., Luke, W. T., Nunnermacker, L. J., Pickering, K. E., Leslie, A. C. D., Lindsey, C. G., Slinn, W. G. N., Kelly, T. J., Daum, P. H., Delaney, A. C., Greenberg, J. P., Zimmerman, P. R., Boatman, J. F., Ray, J. D., and Stedman, D. H.: Thunderstorms: An important mechanism in the transport of air pollutants, Science, 235, 460–465, 1987.

Donner, L. J.: A cumulus parameterization including mass fluxes, vertical momentum dynamics, and mesoscale effects, J. Atmos. Sci., 50, 889–906, 1993.

Dye, J. E., Ridley, B. A., Skamarock, W., Barth, M., Venticinque, M., Defer, E., Blanchet, P., Thery, C., Laroche, P., Baumann, K., Hubler, G., Parrish, D. D., Ryerson, T., Trainer, M., Frost, G., Holloway, J. S., Matejka, T., Bartels, D., Fehsenfeld, F. C., Tuck, A., Rutledge, S. A., Lang, T., Stith, J., and Zerr, R.: An overview of the Stratospheric-Tropospheric Experiment: Radiation, Aerosols, and Ozone (STERAO)-deep convection experiment with results for the July 10, 1996 storm, J. Geophys. Res.,

105, 10 023–10 045, 2000.

Fehr, T., Höller, H., and Huntrieser, H.: Model study on production of lightning-produced NO_x in a EULINOX supercell storm, J. Geophys. Res., 109, D09102, doi:10.1029/2003JD003935, 2004.

Franzblau, E. and Popp, C. J.: Nitrogen oxides produced from lightning, J. Geophys. Res., 94, 11 089–11 104, 1989.

Gallardo, L. and Cooray, V.: Could cloud-to-cloud discharges be as effective as cloud-to-ground discharges in producing NO_x?, Tellus, 48B, 641–651, 1996.

Ganzeveld, L. and Lelieveld, J.: Dry deposition parameterization in a chemistry general circulation model and its influence on the distribution of reactive trace gases, J. Geophys. Res., 100, 20 999–21 012, 1995.

Gidel, L. T.: Cumulus cloud transport of transient tracers, J. Geophys. Res., 88, 6587–6599, 1983.

Heymsfield, A. J., Johnson, P. N., and Dye, J. E.: Observations of moist adiabatic ascent in northeast Colorado cumulus congestus clouds, J. Atmos. Sci., 35, 1689–1703, 1978.

Holton, J. R., Haynes, P. H., McIntyre, M. E., Douglass, A. R., Rood, R. B., and Pfister, L.: Stratosphere-troposphere exchange, Rev. Geoph., 33, 403–439, 1995.

Huntrieser, H., Schlager, H., Feigl, C., and Höller, H.: Transport and production of NO_x in electrified thunderstorms: Survey of previous studies and new observations at midlatitudes, J. Geophys. Res., 103, 28 247–28 264, 1998.

Kawakami, S., Kondo, Y., Koike, M., Nakajima, H., Gregory, G. L., Sachse, G. W., Newell, R. E., Browell, E. W., Blake, D. R., Rodriguez, J. M., and Merrill, J. T.: Impact of lightning and convection on reactive nitrogen in the tropical free troposphere, Geophys. Res. Lett., 102, 28 367–28 384, 1997.

Kley, D., Crutzen, P. J., Smith, H. G. J., Vömel, H., Oltmans, S. J., Grassl, H., and Ramanathan, V.: Observations of near-zero ozone concentrations over the convective Pacific: Effects on air chemistry, Science, 274, 230–233, 1996.

Kley, D., Smit, H. G. J., Vömel, H., Grassl, H., Ramanathan, V., Crutzen, P. J., Williams, S., Meywerk, J., and Oltmans, S. J.: Tropospheric water-vapour and ozone cross-sections in a zonal plane over the central equatorial Pacific Ocean, Q. J. R. Meteorol. Soc., 123, 2009–2040, 1997.

Labrador, L. J., von Kuhlmann, R., and Lawrence, M. G.: Strong sensitivity of the global mean OH concentration and the tropospheric oxidizing efficiency to the source of NO_x from lightning, Geophys. Res. Lett., 31, L06102, doi:10.1029/2003GL019229, 2004.

Landgraf, J. and Crutzen, P. J.: An efficient method for online calculations of photolysis and heating rates, J. Atmos. Sci., 55, 863–878, 1998.

Lawrence, M. G. and Rasch, P. J.: Tracer transport in deep convective updrafts: Plume ensemble versus bulk formulations, J. Atmos. Sci., 62, 2880–2894, 2005.

Lawrence, M. G., Crutzen, P. J., and Rasch, P. J.: Analysis of the CEPEX ozone data using a 3D chemistry-meteorology model, Q. J. R. Meteorol. Soc., 125, 2987–3009, 1999a.

Lawrence, M. G., Crutzen, P. J., Rasch, P. J., Eaton, B. E., and Mahowald, N. M.: A model for studies of tropospheric photochemistry: Description, global distributions, and evaluation, J. Geophys. Res., 104, 26 245–26 277, 1999b.

Lawrence, M. G., von Kuhlmann, R., Salzmann, M., and Rasch, P. J.: The balance of effects of deep convective mixing on tropospheric ozone, Geophys. Res. Lett., 30, 1940, doi:10.1029/2003GL017644, 2003.

Lelieveld, J. and Crutzen, P. J.: Role of deep cloud convection in the ozone budget of the troposphere, Science, 264, 1759–1761, 1994.

Madden, R. A. and Julian, P. R.: Observations of the 40–50 day tropical oscillation – A review, Mon. Weather Rev., 122, 814–837, 1994.

Mahowald, N. M., Rasch, P. J., and Prinn, R. G.: Cumulus parameterizations in chemical transport models, J. Geophys. Res., 100, 26 173–26 189, 1995.

McBride, J. L., , Puri, K., Davidson, N. E., and Tyrell, G. C.: The flow during TOGA COARE as diagnosed by the BMRC tropical analysis and prediction system, Mon. Weather Rev., 123, 717–736, 1995.

Newell, R. E., Wu, Z.-X., Zhu, Y., Hu, W., Browell, E. V., Gregory, G. L., Sachse, G. W., Collins Jr., J. E., Kelly, K. K., and Liu, S. C.: Vertical fine-scale atmospheric structure measured from NASA DC-8 during PEM-West A, J. Geophys. Res., 101, 1943–1960, 1996.

Newell, R. E., Thouret, V., Cho, J. Y. N., Stoller, P., Marenco, A., and Smit, H. G.: Ubiquity of quasi-horizontal layers in the troposphere, Nature, 398, 316–319, 1999.

Orville, R. E., Zisper, E. J., Brook, M., Weidman, C., Aulich, G., Krider, E. P., Christian, H., Goodman, S., Blakeslee, R., and Cummins, K.: Lightning in the region of the TOGA COARE, Bull. Am. Met. Soc., 78, 1055–1067, 1997.

Petersen, W. A., Rutledge, S. A., and Orville, R. E.: Cloud-to-ground lightning observations from TOGA COARE: Selected results and lightning location algorithms, Mon. Weather Rev., 124, 602–620, 1996.

Phillips, V. T. J. and Donner, L. J.: Cloud microphysics, radiation and vertical velocities in two- and three-dimensional simulations of deep convection, Q. J. R. Meteorol. Soc., 132, 3011–3033, 2006.

Pickering, K. E., Thompson, A. M., Dickerson, R. R., Luke, W. T., McNamara, D. P., Greenberg, J. P., and Zimmerman, P. R.: Model calculations of tropospheric ozone production potential following observed convective events, J. Geophys. Res., 95, 14 049–14 062, 1990.

Pickering, K. E., Thompson, A. M., Tao, W.-K., and Kucsera, T. L.: Upper tropospheric ozone production following mesoscale convection during STEP/EMEX, J. Geophys. Res., 98, 8737–8749, 1993.

Pickering, K. E., Thompson, A. M., Wang, Y., Tao, W.-K., McNamara, D. P., Kirchhoff, V. W. J. H., Heikes, B. G., Sachse, G. W., Bradshaw, J. D., Gregory, G. L., and Blake, D. R.: Convective transport of biomass burning emissions over Brazil during TRACE A, J. Geophys. Res., 101, 23 993–24 012, 1996.

Pickering, K. E., Wang, Y., Tao, W.-K., Price, C., and Müller, J.-F.: Vertical distributions of lightning NO_x for use in regional and global chemical transport models, J. Geophys. Res., 103, 31 203–31 216, 1998.

Pickering, K. E., Thompson, A. M., Kim, H., DeCaria, A. J., Pfister, L., Kucsera, T. L., Witte, J. C., Avery, M. A., Blake, D. R., Crawford, J. H., Heikes, B. G., Sachse, G. W., Sandholm, S. T., and Talbot, R. W.: Trace gas transport and scavenging in PEM-Tropics B South Pacific Convergence Zone convection, J. Geophys. Res., 106, 32 591–32 602, 2001.

Poulida, O., Dickerson, R. R., and Heymsfield, A.: Stratosphere-troposphere exchange in a midlatitude mesoscale convective complex, J. Geophys. Res., 101, 6823–6836, 1996.

Price, C. and Rind, D.: A simple lightning parameterization for calculating global lightning distributions, J. Geophys. Res., 97, 9919–9933, 1992.

Price, C. and Rind, D.: What determines the cloud-to-ground lightning fraction in thunderstorms?, Geophys. Res. Lett., 20, 463–466, 1993.

Price, C., Penner, J., and Prather, M.: NO_X from lightning: 1. Global distribution based on lightning physics, J. Geophys. Res., 102, 5929–5941, 1997.

Ramanathan, V. R., Dirks, R., Grossman, R., Heymsfield, A., Kuettner, J., and Valero, F. P. J.: Central Equatorial Pacific design, Center for Clouds, Chemistry, and Climate, University of California, San Diego, 1993.

Ray, P. S., MacGorman, D. R., Rust, W. D., Taylor W. L., and Walters Rasmussen, L.: Lightning location relative to storm structure in a supercell and a multicell storm, J. Geophys. Res., 92, 5713–5724, 1987.

Redelsperger, J., Brown, P. R. A., Guichard, F., Hoff, C., Kawasima, M., Lang, S., Montmerle, T., Nakamura, K., Saito, K., Seman, C., Tao, W.-K., and Donner, L. J.: A GCSS model intercomparison for a tropical squall line observed during TOGA-COARE. I: Cloud-resolving models, Q. J. R. Meteorol. Soc., 26, 823–863, 2000.

Salzmann, M.: Influences of deep convective cloud systems on tropospheric trace gases and photochemistry over the tropical West Pacific: A modeling case study, Ph.D. thesis, Johannes Gutenberg-Universität Mainz, Mainz, Germany, http://nbn-resolving.de/urn/resolver.pl?urn=urn:nbn:de:hebis:77-9470, 2005.

Salzmann, M., Lawrence, M. G., Phillips, V. T. J., and Donner, L. J.: Modelling tracer transport by a cumulus ensemble: Lateral boundary conditions and large-scale ascent, Atmos. Chem. Phys., 4, 1797–1811, 2004, http://www.atmos-chem-phys.net/4/1797/2004/.

Salzmann, M., Lawrence, M. G., Phillips, V. T. J., and Donner, L. J.: Model sensitivity studies regarding the role of the retention coefficient for the scavenging and redistribution of highly soluble trace gases by deep convective cloud systems., Atmos. Chem. Phys., 7, 2027–2045, 2007.

Sander, R. and Crutzen, P. J.: Model study indicating halogen activation and ozone destruction in polluted air masses transported to the sea, J. Geophys. Res., 101, 9121–9138, 1996.

Scala, J. R., Garstang, M., Tao, W.-K., Pickering, K. E., Thompson, A. M., Simpson, J., Kirchhoff, V. W. J. H., Browell, E. V., Sachse, G. W., Torres, A. L., Gregory, G. L., Rasmussen, R. A., and Khalil, M. A. K.: Cloud draft structures and trace gas transport, J. Geophys. Res., 95, 17 015–17 030, 1990.

Schumann, U. and Huntrieser, H.: The global lightning-induced nitrogen oxides source, Atmos. Chem. Phys., 7, 3823–3907, 2007, http://www.atmos-chem-phys.net/7/3823/2007/.

Skamarock, W. C., Klemp, J. B., and Dudhia, J.: Prototypes for the WRF (Weather Research and Forecasting) model, in: Preprints, Ninth Conf. Mesoscale Processes, pp. J11–J15, Amer. Meteor. Soc., Fort Lauderdale, FL, 2001.

Skamarock, W. C., Dye, J. E., Barth, M. C., Stith, J. L., Ridley, B. A., and Baumann, K.: Observational- and modeling-based budget of lightning-produced NO_X in a continental thunderstorm, J. Geophys. Res., 108, 4035, doi:10.1029/2002JD002163, 2003.

Stenchikov, G., Dickerson, R., Pickering, K., Ellis Jr., W., Doddridge, B., Kondragunta, S., Poulida, O., Scala, J., and Tao, W.-K.: Stratosphere-troposphere exchange in a midlatitude mesoscale convective complex, 2. Numerical simulations, J. Geophys. Res., 101, 6837–6851, 1996.

Takemi, T. and Rotunno, R.: The effects of subgrid model mixing and numerical filtering in simulations of mesoscale cloud systems, Mon. Weather Rev., 131, 2085–2191, 2003.

von Kuhlmann, R., Lawrence, M. G., Crutzen, P. J., and Rasch, P. J.: A model for studies of tropospheric ozone and nonmethane hydrocarbons: Model description and ozone results, J. Geophys. Res., 108, doi:10.1029/2002JD002893, 2003.

Walcek, C. J.: Minor flux adjustment near mixing ratio extremes for simplified yet highly accurate monotonic calculation of tracer advection, J. Geophys. Res., 105, 9335–9348, 2000.

Wang, C. and Chang, J. S.: A three-dimensional numerical model of cloud dynamics, microphysics, and chemistry: 3. Redistribution of pollutants, J. Geophys. Res., 98, 16 787–16 798, 1993.

Wang, C. and Prinn, R. G.: On the roles of deep convective clouds in tropospheric chemistry, J. Geophys. Res., 105, 22 269–22 297, 2000.

Wang, C., Crutzen, P. J., Ramanathan, V., and Williams, S. F.: The role of a deep convective storm over the tropical Pacific Ocean in the redistribution of atmospheric chemical species, J. Geophys. Res., 100, 11 509–11 516, 1995.

Webster, P. J. and Lukas, R.: TOGA COARE: The Coupled Ocean-Atmosphere Response Experiment, Bull. Am. Met. Soc., 73, 1377–1416, 1992.

Wild, O.: Modelling the global tropospheric ozone budget: exploring the variability in curerent models, Atmos. Chem. Phys., 7, 2643–2660, 2007, http://www.atmos-chem-phys.net/7/2643/2007/.

Yanai, M., Chen, B., and Tung, W.-W.: The Madden-Julian Oscillation observed during the TOGA COARE IOP: Global view, J. Atmos. Sci., 57, 2374–2396, 2000.